The Radiological Footprint of a Be-based Neutron Source

by
Sharareh Koufigar
Supervisor: Dr. Kevin Fissum

Division of Nuclear Physics
Department of Physics
Lund University

Spring 2015
FYSK01

LUND
UNIVERSITY

Abstract

The radiological footprint of a Be-based neutron source embedded within the Aquarium of the Source-Testing Facility (STF) at the Division of Nuclear Physics at Lund University will soon be carefully mapped. As a precursor to this measurement program, neutron and gamma-ray energy spectra at beamport apertures have been measured using ^{3}He and $LaBr_3$(Ce) (cerium-activated lanthanum bromide) detectors. The measured energy spectra and rates will provide crucial benchmarks for ongoing efforts to simulate the neutron and gamma-ray fields associated with the source. The ultimate goal of the project is the development of a software toolkit which precisely replicates the radiological environment provided by the source. This toolkit will greatly facilitate the interpretation of detector-development and shielding studies performed at the STF.

Abbreviations

CAD	Computer-Aided Design
ESS	European Spallation Source
FWHM	Full-Width-at-Half-Maximum
MCA	Multi-Channel Analyzer
PMMA	Poly-Methyl-Methacrylate
PMT	Photomultiplier Tube
STF	Source-Testing Facility
$LaBr_3(Ce)$	Cerium-activated lanthanum bromide

Contents

List of Figures

List of Tables

Chapter 1

Introduction

In 1911, Rutherford first proposed that atoms consist of a small heavy nucleus with positive charge and a cloud of light negatively charged particles. In 1920, he further suggested that there were neutral particles in the nucleus of an atom, which were the result of protons and electrons binding in some unknown way. He named these uncharged particles "neutrons". In 1931, Walther Bothe and Herbert Becker discovered that if a beryllium plate was bombarded by alpha particles, an unusual penetrating radiation was obtained. This radiation was assumed to be gamma radiation until 1932, when James Chadwick determined that the new radiation consisted of uncharged particles having about the same mass as the proton.

The neutron is a subatomic particle with no electric charge that is composed of three quarks: one "up" quark and two "down" quarks (see Fig. 1.1). The strong force holds these quarks together to form both protons and neutrons.

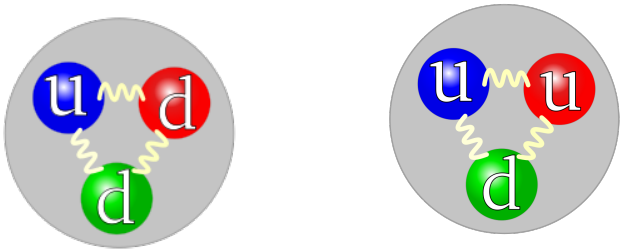

(a) (b)

Figure 1.1: Quark Structure of the Neutron and the Proton. (a) the neutron; (b) the proton. "u" represents an "up" quark, and "d" represents a "down" quark. The "springs" represent the binding between the quarks. Figure from Ref. [1].

An atomic nucleus consists of protons and neutrons which are held together by two forces that counterbalance each other. The attractive strong force acts between all nucleons over a

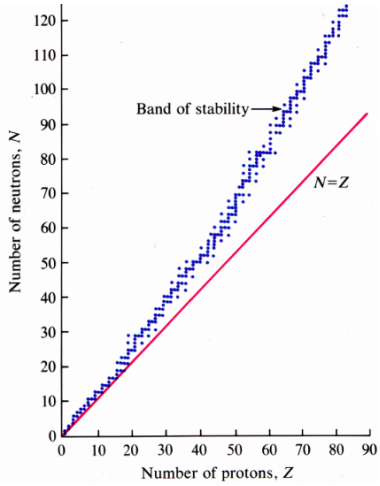

Figure 1.2: Nuclear Stability Graph. The number of neutrons has been plotted against the number of protons in the nucleus for many elements. The dots represent stable nuclei while the red line illustrates an equal number of neutrons and protons. An excess of neutrons exists in all but the very lightest nuclei. Figure from Ref. [2].

distance of about 1 fm[1]. The repulsive Coulomb force acts between all protons over an infinite distance. A stable system of many protons and neutrons can result if the attractive strong force between the nucleons overcomes the repulsive Coulomb force between the protons [3].

Neutrons that are bound within an atomic nucleus are stable. As an illustration of the importance of the neutron to matter, Fig. 1.2 illustrates the stability of the elements. It is clear that for most atomic nuclei, there are more neutrons than protons present in the nucleus. Bound neutrons are thus crucial to the existence of the elements as we know them. Neutrons that are outside of the atomic nucleus (free neutrons) are unstable and have a mean life time of about 15 minutes [4]. The β^- decay of the neutron is given by

$$n \rightarrow p + e^- + \bar{\nu}_e, \tag{1.1}$$

where n is the neutron, p is a proton, e^- is an electron, and $\bar{\nu}_e$ is an electron-associated antineutrino. The Q-value of this process is (0.782 ± 0.013) MeV [5]. The Q-value is the mass difference between the initial and final states. It represents the energy released in the decay. This energy is shared kinetically by the particles in the final state.

Due to their lack of charge, free neutrons are deeply penetrating probes of matter. They are used in many diverse applications from imaging, to diagnostic tools, to homeland security. Free neutrons originate from many different processes. Environmental neutrons are produced when cosmic rays interact with the upper atmosphere. Neutrons may also be produced by nuclear reactors, particle accelerators, and radioactive sources. Of these, radioactive sources have by far the lowest cost per neutron. Two types of radioactive sources which produce free neutrons are spontaneous fission sources such as ^{252}Cf and beryllium-based sources such as ^{241}Am/Be, $^{239/238}$Pu/Be and ^{226}Ra/Be.

In this thesis, the radiological footprint of a Be-based source was investigated as the first step towards calibrating the Source-Testing Facility (STF) at the Division of Nuclear Physics at Lund University. The measurements performed here shall provide valuable information

[1] 1 fm $= 10^{-15}$ m.

about the source-associated neutron and gamma-ray rates and energy distributions. This in turn will enable simulations of the neutron and gamma-ray fields associated with the source using such toolkits as Geant4 [6], MCNPX [7], McStas [8], and Stanton [9]. The ultimate goal of the project is to develop a precision software toolkit capable of reproducing the radiological environment provided by the Be-based source. This toolkit will greatly simplify the interpretation of data obtained for detector development and shielding studies obtained with it.

Chapter 2

Materials and Methods

2.1 Be-based Neutron Source

The free-neutron production mechanism for a Be-based source relies upon the actinide-associated alpha particle. Free neutrons are produced according to the reaction illustrated in Eq. 2.1. When the alpha particles react with ^{9}Be, ^{12}C and a free neutron are produced. Depending on the reaction kinematics, the ^{12}C nucleus may be left in its ground, first, or second excited state according to

$$\alpha + {}^{9}\mathrm{Be} \rightarrow \begin{cases} {}^{12}\mathrm{C} + n & \text{(ground state)} \\ {}^{12}\mathrm{C}^{*} + n & \text{(first-excited state) at 4.44 MeV} \\ {}^{12}\mathrm{C}^{**} + n & \text{(second-excited state) at 7.65 MeV.} \end{cases} \tag{2.1}$$

The Q-value of the alpha decay of the original radioisotope is on average about 5.5 MeV. This appears as kinetic energy of the alpha particle. The Q-value of α + ^{9}Be $\rightarrow$ ^{12}C + n reaction to the ground state is 5.7 MeV. Thus, there are at most roughly 11 MeV of energy to be shared by the reaction products [10]. The relative populations of the ground state, the first-excited state, and the second-excited state for the recoiling ^{12}C nucleus are a function of the energy of the neutron emitted. For example, for the alpha emitter ^{238}Pu/Be, the populations are $\sim$33%, $\sim$60%, and $\sim$7% respectively (see Fig. 2.1). Note that when ^{12}C de-excites from the first excited state to the ground state, a 4.44 MeV gamma-ray is released.

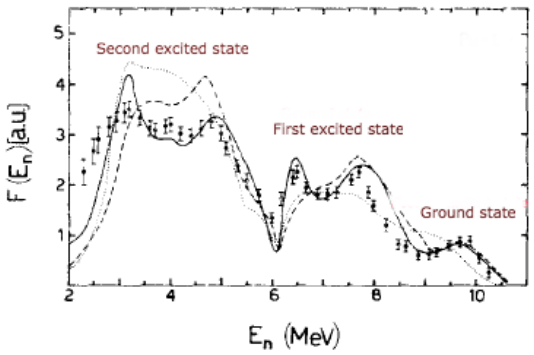

Figure 2.1: Free-Neutron Distributions. A comparison of the relative populations of the ground, first-excited, and second-excited states in ^{12}C for ^{238}Pu/Be. Neutrons with energies from 2 MeV to 11 MeV are emitted. Figure from Ref. [11].

The source employed for this project was a mixture of an α-emitter and ^{9}Be ceramic encapsulated in a stainless-steel X.3 capsule (see Fig. 2.2). It was determined on August 29, 1973 to have an activity of 185 GBq, which resulted in $(4.21\pm0.01) \cdot 10^{6}$ neutrons per second being emitted nearly isotropically [12].

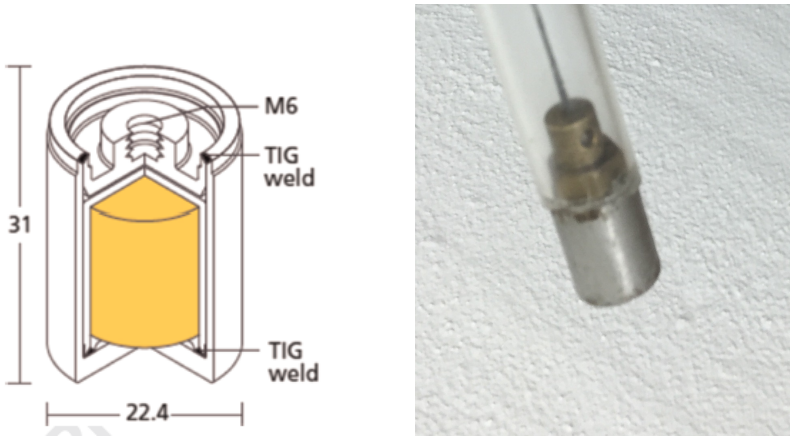

(a) (b)

Figure 2.2: The Source. (a) schematic drawing (dimensions are given in mm). The yellow volume in the center is the radioactive material; (b) photograph. Figure (a) from Ref. [12]. Photograph by the author.

2.2 Source Tank

The Division of Nuclear Physics at Lund University hosts a Source-Testing Facility (STF) for neutron-detector characterization and shielding tests. The main component of the STF is the Aquarium, a movable water-shielded tank designed specifically for producing beams of neutrons and gamma-rays from Be-based sources (see Fig. 2.3).

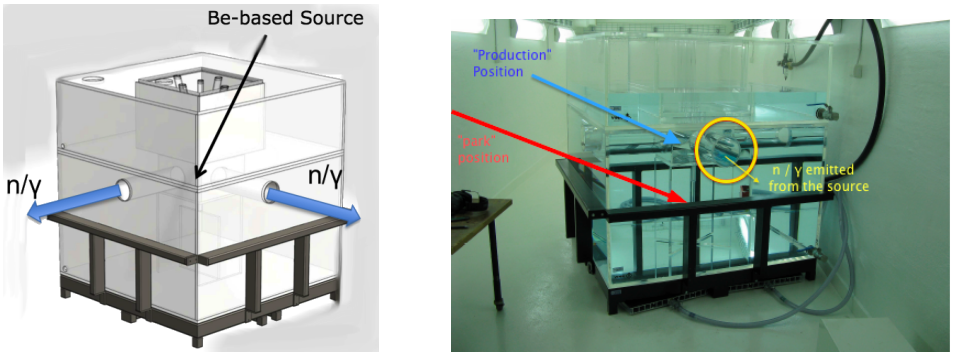

(a) (b)

Figure 2.3: The Source Tank. (a) Computer-Aided Design (CAD) image; (b) photograph. The red and yellow arrows indicate the source "park" and "production" positions, respectively. The neutron/gamma-ray beams are also indicated. Figure (a) is from Ref. [13]. Photograph by the author.

The Aquarium is mounted on a steel support frame and the entire system may be moved using air pads via a 6 bar pressurized air system. The tank itself is made of poly-methyl-methacylate (PMMA), also known as plexiglass or lucite, and was produced by VINK [14]. The tank has outer dimensions of 140 cm × 140 cm × 140 cm. It is filled with approximately 2650 liters of ultra-pure de-ionized water. Four horizontal, cylindrical beamports 172 mm in diameter and 500 mm in length are located on each face of the tank at a height of 110 cm above the floor ("production" height). These ports define beams and allow for four simultaneous and independent irradiations to be performed. Each beamport can also be sealed using a polyethylene plug.

2.3 Detectors

2.3.1 $LaBr_3$(Ce) Gamma-ray Detector

The scintillation process is one of the most useful processes available for detecting ionizing radiation. Scintillation material converts the energy of the incident radiation into detectable light. The most widely used scintillators today are inorganic alkali halide crystals such as NaI(TI) and organic-based plastics such as NE102 [15]. Inorganic scintillators tend to have the best light output and linearity but they are slow in their rise time[1] (2.4 ns for NE102 versus 230 ns for NaI(TI)). They are mainly used for photon detection because of their high density and high average Z-value[2] which make them particularly sensitive [15].

[1]The rise time represents the quickness of the detector to react to the incident radiation. The shorter the rise time, the faster the response.

[2]The Z-value is also known as the atomic number. It represents the number of protons in the nucleus.

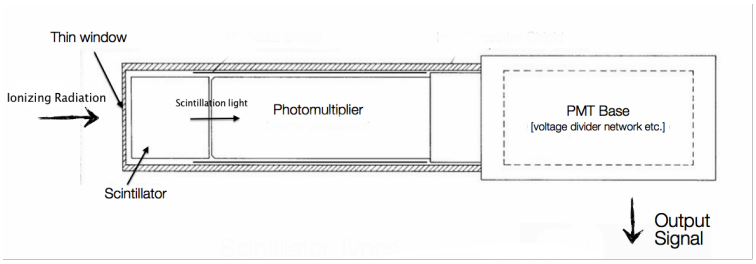

Figure 2.4: Scintillators – Basic Counter Setup. Incident ionizing radiation is converted to an output signal. Figure from Ref. [16].

As Fig. 2.4 illustrates, ionizing radiation incident upon a scintillator results in flashes of light which are directed towards a photomultiplier tube (PMT). PMTs convert the scintillation light into an output signal. An illustration of a PMT is presented in Fig. 2.5.

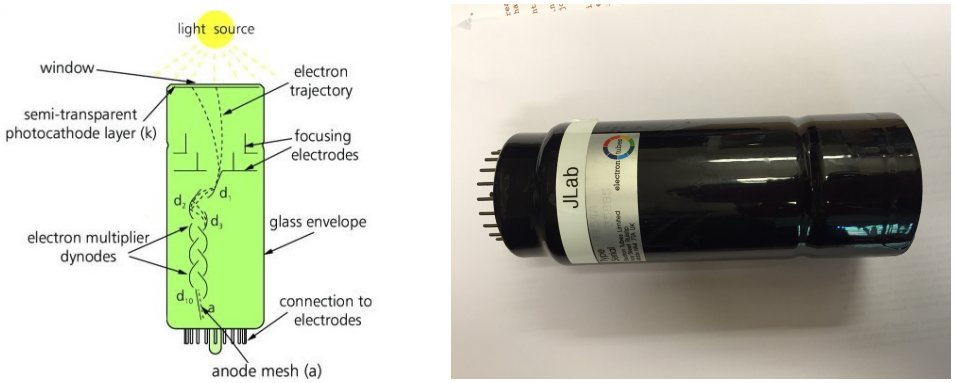

(a) (b)

Figure 2.5: Photomultiplier Tube. (a) generic illustration; (b) photograph. Figure from Ref. [17]. Photograph by author.

PMTs often receive scintillation light through a hard optical window such as borosilicate glass [18]. This hard window covers a photosensitive surface called a "photocathode". At the photocathode, the light produced in the scintillator is converted to electrons via the photoelectric effect[3]. These photoelectrons are then electrostatically accelerated and focused onto electrodes known as the "dynodes". At each dynode, more and more electrons are released. At the end of the dynode chain there is a collection electrode known as the "anode". The resulting pulse of electrons on the anode is proportional to the energy of the incident radiation.

Cerium-activated lanthanum bromide ($LaBr_3(Ce)$) is a new inorganic scintillator optimized for gamma-ray detection that is in high demand. It has a fast rise time of 16 ns [19], a short decay time[4] of 0.026 μs[5] [20], and provides excellent energy resolution (see Sec. 2.3.3)

[3]Electrons are freed from the surface of a metal due to the energy of the incident photons.
[4]The short decay time means that the crystal is able to react to the next incident gamma-ray very quickly.
[5]1 μs = 10^{-6} s.

[15]. A useful feature of this scintillator is the intrinsic radioactivity of ^{138}La which can be used for energy calibration [21]. ^{138}La has two main decay modes: electron capture to ^{138}Ba (66.4%), which results in a 1.44 MeV gamma-ray, and β^- decay (33.6%) with a 0.225 MeV endpoint energy [15]. The $LaBr_3$(Ce) detector employed in this work was a 1.5" $\times$ 1.5" cylindrically shaped crystal connected to a 1.5" diameter PMT (see Fig. 2.6) operated at +775 V. It was provided by the Detector Group of the European Spallation Source (ESS). It generated analog signals with negative amplitude. These analog signals were inverted and amplified before being passed to a multi-channel analyzer (MCA) to be digitized and eventually histogrammed.

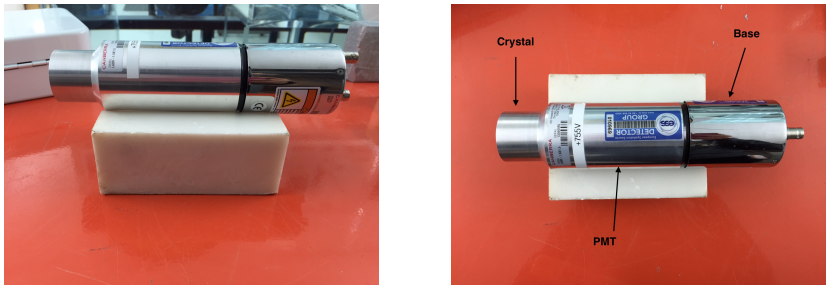

(a) (b)

Figure 2.6: $LaBr_3$(Ce) Detector. (a) side view; (b) top view. Photographs by author.

2.3.2 ^{3}He-based Neutron Detector

Similar to gamma rays, neutrons carry no charge; therefore, they can be difficult to detect. Depending upon their energy, neutrons are detected via different interaction mechanisms. Neutron interaction mechanisms include nuclear reactions and scattering. When neutrons undergo nuclear reactions, secondary radiations result which are almost always heavier charged particles. When neutrons scatter, their direction and energy can change significantly. It is the recoiling charged particle that is detected.

Most detectors of low-energy neutrons first convert the incident neutron into secondary charged particles which can be detected directly [15]. This converter is often a noble gas[6], and these detectors are called "proportional counters". The key feature of these detectors is their ability to measure the energy of the secondary radiation by producing a signal that is proportional to it. A very common gas used for detecting thermal neutrons is ^{3}He. The ^{3}He gas acts as a conversion medium according to

$$n + {}^3\mathrm{He} \rightarrow {}^3\mathrm{H} + p + 0.764\,\mathrm{MeV}, \tag{2.2}$$

where n is the neutron, ^{3}H is tritium, and p is the proton. The recoiling p and ^{3}H ionize the surrounding gas atoms, which in turn ionize other gas atoms in an avalanche-like multiplication process. The resulting ionization is collected as an electrical pulse. This pulse has an

[6]Noble gases are chemically inactive. They are colorless and tasteless. They are also non-flammable.

amplitude and integral proportional to the energy deposited by the p and the ^{3}H in the gas.

A pulse-height energy spectrum that serves as a "fingerprint" for the identification of the thermal neutrons by a ^{3}He detector is shown in Fig. 2.7 [22].

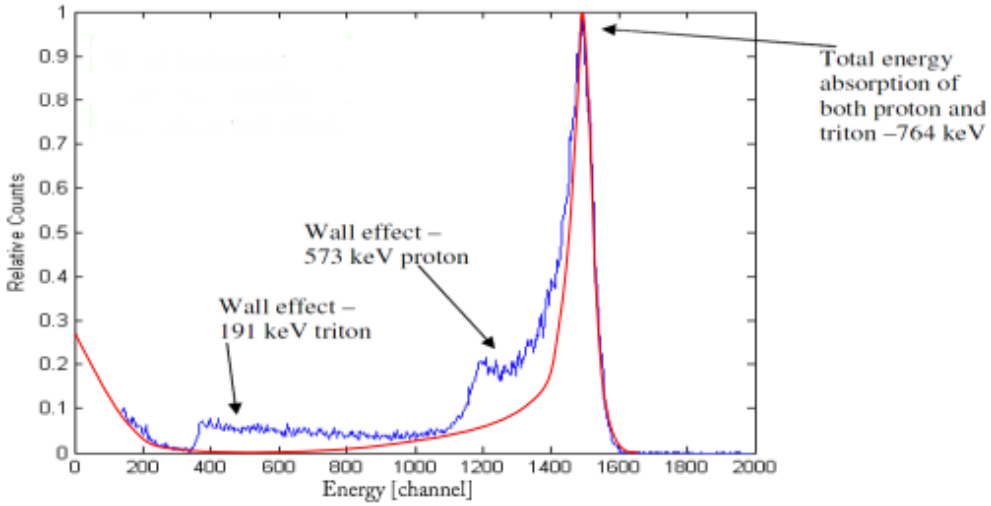

Figure 2.7: Typical ^{3}He Spectrum. Energy spectrum for thermal neutrons incident on a ^{3}He detector. The peak at 0.764 MeV corresponds to both the p and ^{3}H depositing all of their kinetic energy in the gas. Wall effects (see text) are also shown. Figure from Ref. [22].

If the entire energy of the reaction products is completely deposited within the ^{3}He gas, the "full-energy" peak results. This full-energy peak occurs at 0.764 MeV [15]. "Wall effects" arise because the p and/or ^{3}H reaction products collide with the wall of the detector. In this case, the full energy of the reaction is not deposited in the ^{3}He gas but rather some of it ends up in the detector walls. If the ^{3}H strikes the wall, a step appears at 0.191 MeV. If the p strikes the wall, a step appears at 0.573 MeV. A smaller detector shows greater effects from the walls since fewer particles can deposit all of their kinetic energy in the smaller gas volume before they hit the walls. The ^{3}He proportional counter used in this work was a 1" $\times$ 10" cylinder loaded with 10 bar (or 10^6 Pa) of ^{3}He (see Fig. 2.8). It was provided by the Detector Group of the ESS.

Figure 2.8: ^{3}He Proportional Counter. Top-view. Photograph by author.

2.3.3 Energy Resolution

The energy resolution of a detector refers to its ability to precisely measure the energy of the incident ionizing radiation. Consider a very large number of ionizing radiation events of energy E incident upon a detector. Based upon the resolution of the detector, sometimes the detected energy will be less than E, sometimes it will be more than E, and sometimes it will be exactly E. The energy resolution of a detector may be determined by the width of this so-called "monochromatic" peak. It is common to use the Full-Width-at-Half-Maximum (FWHM) of this peak when expressing the energy resolution of a detector. Measured FWHM is the width of the peak at half of the highest point of the corresponding measured normal or Gaussian distribution. The energy resolution is given by

$$R = \frac{\Delta E_{\mathrm{FWHM}}}{E}, \tag{2.3}$$

where ΔE_{FWHM} is the FWHM in units of energy, and E is the energy of the peak (see Fig. 2.9). In general, the lower the value of R, the better the resolution of the detector.

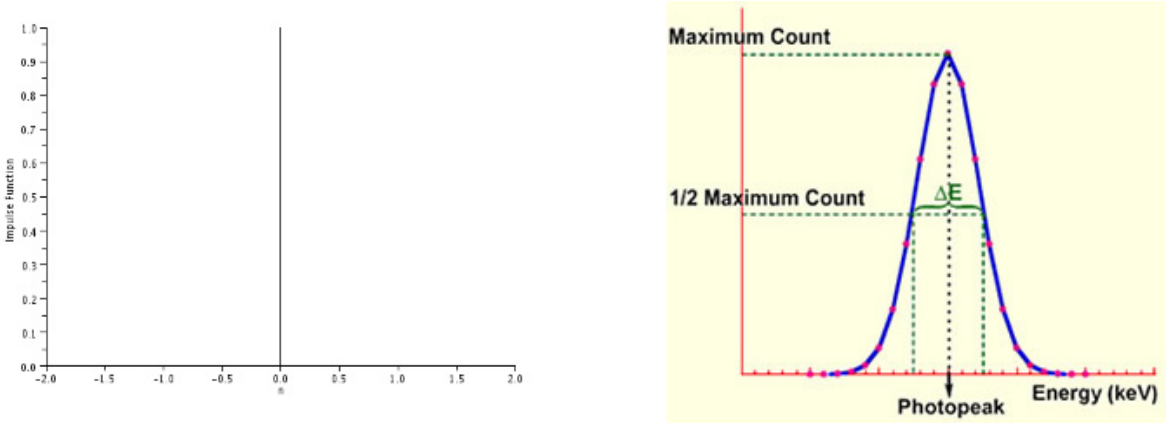

(a) (b)

Figure 2.9: Energy Resolution. (a) incident energy distribution (monoenergetic), a delta-function; (b) detected energy distribution, a Gaussian function. Figures (a) and (b) from Refs. [23] and [24], respectively.

Chapter 3

Results and Discussion

Measurements were performed to obtain neutron and gamma-ray spectra from a Be-based source for various source/detector combinations and configurations. The location of the source was varied between so-called "production" position (where it was carefully aligned with the penetrations in the water tank to purposefully allow for the maximum number of gamma-rays and neutrons to escape the Aquarium) and so-called "park" position (where the amount of water shielding between the source and the detector in question was maximized). The locations of the $LaBr_3$(Ce) gamma-ray and ^{3}He neutron detectors were also varied between these positions (see Fig. 3.1). By carefully analyzing the resulting data, benchmarks were obtained which are in principle very simple to simulate. This will facilitate the software modeling of the radiological footprint of the Be-based source, which will in turn ease the interpretation of detector-development and shielding studies performed with it.

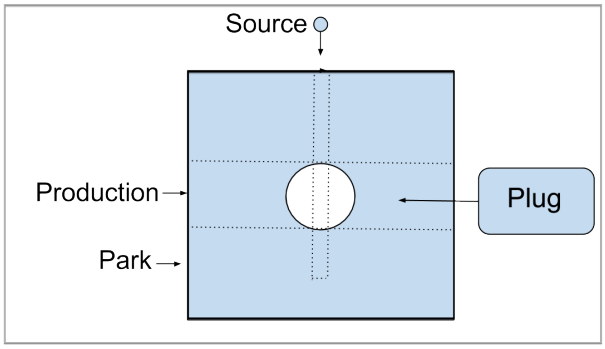

Figure 3.1: Drawing of the Source Tank. Side-view. The "park" and "production" positions together with the source and plug penetrations are indicated. Drawing by author.

3.1 $LaBr_3$(Ce) Gamma-ray Detector

3.1.1 Calibration

Three well-known gamma-ray sources were used to calibrate the $LaBr_3$(Ce) detector: ^{60}Co, ^{137}Cs, and ^{22}Na. The gamma-ray energies corresponding to these sources are shown in Table 3.1. The intrinsic activity of ^{138}La was also used as a calibration point.

Table 3.1: Gamma-ray Sources and Corresponding Energies. Gamma-ray energies taken from Ref. [15].

Source	γ_1 Energy (MeV)	γ_2 Energy (MeV)
^{60}Co	1.17	1.33
^{137}Cs	0.662	
^{22}Na	0.511	1.27
^{138}La	1.45	

In each case, the source in question was placed in front of the $LaBr_3$(Ce) detector and a 30 min irradiation was performed. Peaks associated with the gamma-rays coming from the sources and the intrinsic radioactivity of the $LaBr_3$(Ce) detector were clearly identified. The results are presented in Fig. 3.2.

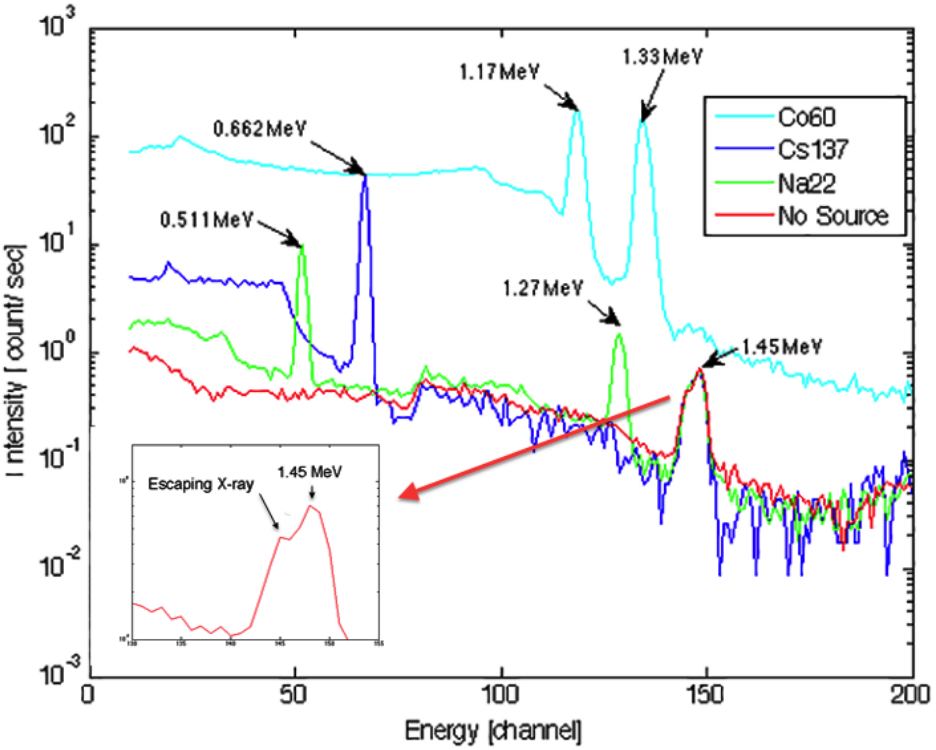

Figure 3.2: Uncalibrated $LaBr_3(Ce)$ Detector Energy Spectrum. Time-normalized, non-calibrated gamma-ray spectra obtained using various gamma-ray sources and the $LaBr_3(Ce)$ detector. The peaks associated with the gamma-rays are identified. The plot in the bottom left-hand corner details the peak resulting from the intrinsic activity of ^{138}La.

The ^{138}La-associated peak is the result of electron capture to $^{138}Ba^*$ which results in both a 1.44 MeV gamma-ray and a simultaneous 0.032 MeV X-ray from the decay of $^{138}Ba^*$. If this X-ray escapes detection, then 1.44 MeV and not 1.45 MeV are deposited [15].

Table 3.2 shows the gamma-ray energies corresponding to each calibration source together with the position of the corresponding gamma-ray peak in Fig. 3.2.

Table 3.2: $LaBr_3(Ce)$ Detector Energy Calibration.

Source	Gamma-ray Energy (MeV)	Channel Number
^{22}Na	0.511	52
^{137}Cs	0.622	67
^{60}Co	1.17	118
^{22}Na	1.27	129
^{66}Co	1.33	134
^{138}La	1.45	148

These values were used to calibrate the $LaBr_3(Ce)$ detector for energy. Fig. 3.3 illustrates the energy calibration of the $LaBr_3(Ce)$ detector. The gamma-ray peak energies have been plotted against gamma-ray peak positions for each of the sources detailed in Table 3.2. A linear function was then fitted to these data.

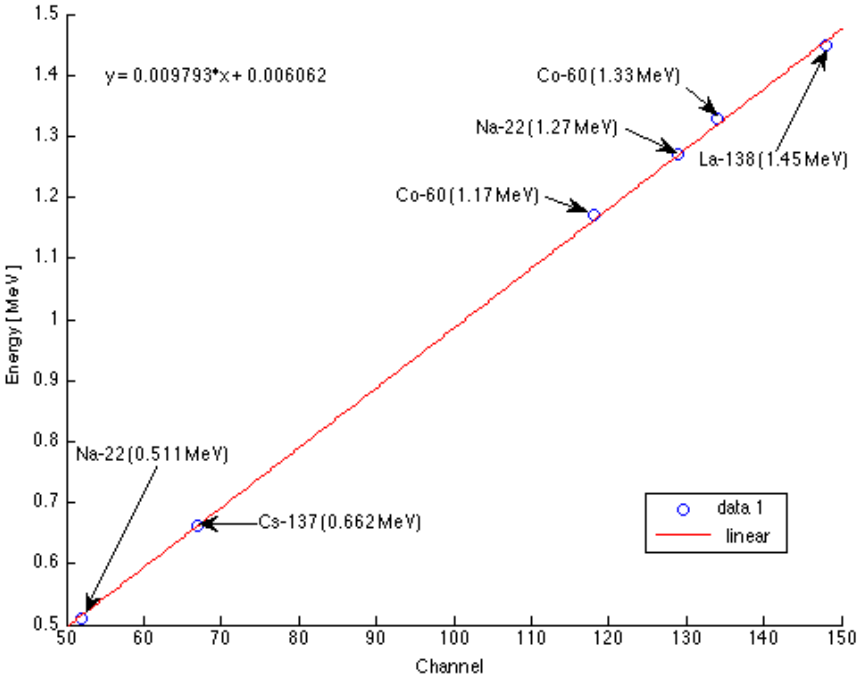

Figure 3.3: Energy Calibration of the $LaBr_3(Ce)$ Detector. The energies of the gamma-rays coming from the various sources and the $LaBr_3(Ce)$ detector have been plotted against the corresponding measured gamma-ray peak positions (open blue circles). A linear fitted energy-calibration relation (red line) is also shown.

The energy calibration relation for the $LaBr_3(Ce)$ detector is given by

$$E_\gamma[\text{MeV}] = m \cdot E_\gamma[\text{channel}] + b, \tag{3.1}$$

where E_γ[MeV] is the energy of the detected event in MeV, m is the slope of the fitted line in $\frac{\text{MeV}}{\text{channel}}$, and b is the offset of the fitted line in MeV. The m value was determined to be 0.009793 $\frac{\text{MeV}}{\text{channel}}$ and b was determined to be 0.006062 MeV. By applying this calibration relation to all of our subsequent $LaBr_3$(Ce) data, energy-calibrated spectra were obtained.

3.1.2 Resolution

The energy resolution of the $LaBr_3$(Ce) detector was studied by examining the widths and positions of the gamma-ray peaks. Figure 3.4 presents a sample overview of the analysis performed. First, a Gaussian function was fitted to a peak. From the fitted function, the location of each peak together with its FWHM was determined. Finally, Eq. 2.3 was employed to calculate the energy resolution. The procedure was repeated for all of the peaks presented in Fig. 3.5. The results are given in Table 3.3, which shows the energy resolution of the $LaBr_3$(Ce) detector as a function of gamma-ray energy.

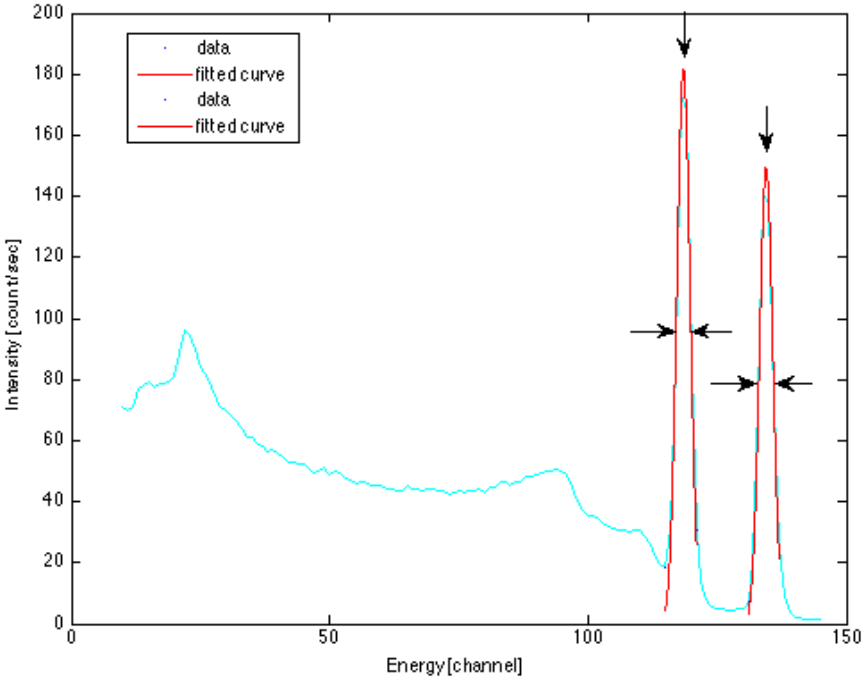

Figure 3.4: Determination of Energy Resolution. A Gaussian function (red line) has been fitted to the data (blue dots) obtained with the ^{60}Co source and $LaBr_3$(Ce) detector. The arrows indicate where the FWHMs and photopeaks are located.

Table 3.3: Energy Resolution of the $LaBr_3(Ce)$ Detector. The energy resolution of the $LaBr_3(Ce)$ detector as a function of gamma-ray energy is shown.

Source	γ Energy (MeV)	μ [channel]	FWHM [channel]	Energy Resolution [%]
^{22}Na	0.511	52	2.71	5.6 ± 0.2
^{137}Cs	0.622	67	2.80	4.2 ± 0.2
^{60}Co	1.17	118	4.26	3.6 ± 0.2
^{22}Na	1.27	129	1.89	3.5 ± 0.2
^{60}Co	1.33	135	4.24	3.2 ± 0.2
n capture by H	2.22	223	6.73	3.0 ± 0.2
de-excitation of $^{12}C^*$	4.44	441	18.40	4.2 ± 0.2

The average energy resolution of the $LaBr_3(Ce)$ detector over the energy range 0.511 MeV to 4.44 MeV was determined to be (3.9 ± 0.3)%.

3.1.3 Be-based Source Gamma-ray Footprint

Subsequent to the energy calibration of the $LaBr_3(Ce)$ detector, a detailed investigation of the gamma-ray footprint of the Be-based neutron source was performed. The Be-based source was placed in both the park position and the production position (see Fig. 3.1). The $LaBr_3(Ce)$ detector was positioned 85 mm from the outside wall of the Aquarium for a total distance of 785 mm from the source. The height of the $LaBr_3(Ce)$ detector was varied between the park position and the production position. Data were obtained with and without a polyethylene plug in the penetration in order to easily vary the rates and increase the dynamics of the dataset.

The data obtained for the various experimental configurations are shown in Fig. 3.5. The key identifies the relative positioning of the source and the detector as well as whether or not the polyethylene plug was in place. Peaks associated with the monoenergetic gamma-rays coming from the Be-based source, the interaction of the neutrons from the Be-based source with the water of the Aquarium and the polyethylene of the plug, and the room background are all clearly identified. Table 3.4 presents a detailed overview of the results.

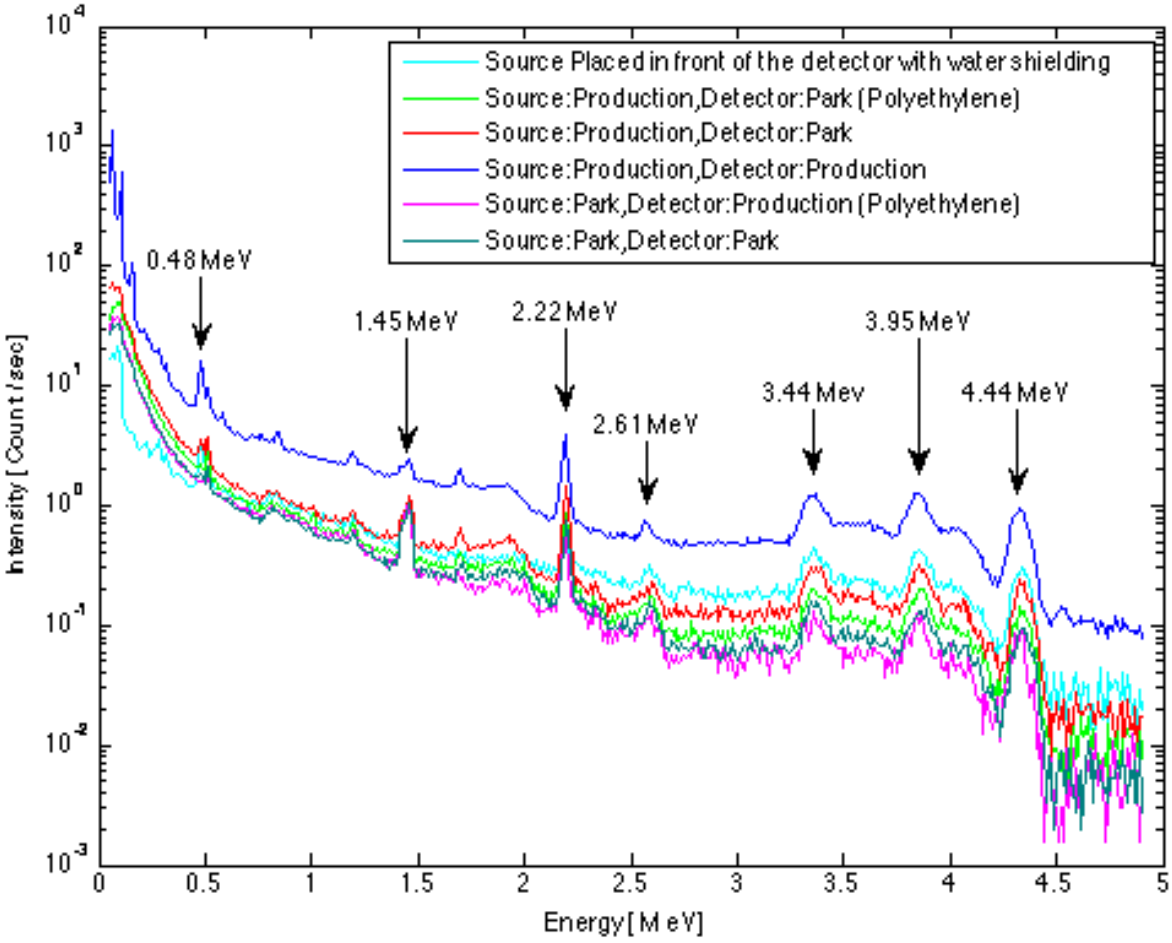

Figure 3.5: Calibrated $LaBr_3(Ce)$ Detector Energy Spectrum. Time-normalized, energy-calibrated gamma-ray spectra obtained using the Be-based source and the $LaBr_3(Ce)$ detector. The peaks are clearly identified. Configurations are defined in the key.

Table 3.4: Calibrated $LaBr_3(Ce)$ Detector Energy Peaks and Their Origin. See text for details.

Energy (MeV)	Source
0.48	Neutron capture by ^{10}B
1.45	Intrinsic activity of ^{138}La
2.22	Neutron capture by hydrogen in paraffin and water
2.61	De-excitation of ^{208}Pb (Th series)
3.44	4.44 MeV double escape
3.95	4.44 MeV single escape
4.44	de-excitation of $^{12}C^*$

Table 3.4 presents a summary of the gamma-ray peaks observed in the $LaBr_3(Ce)$ spectra together with their corresponding origin.

- The peak at 0.48 MeV corresponds to n capture by ^{10}B. ^{10}B was present in the piece of plastic the detector was sitting on (recall Fig. 2.6).
  $n + {}^{10}B \rightarrow {}^{7}Li^* + {}^{4}He \rightarrow {}^{7}Li + \gamma$ (0.48 MeV) + ^{4}He

- The peak at 1.45 MeV corresponds to electron capture by ^{138}La.
  $e^- + {}^{138}La \rightarrow {}^{138}Ba^* \rightarrow {}^{138}Ba + \gamma$ (1.45 MeV)

- The peak at 2.22 MeV corresponds to n capture by ^{1}H in polyethylene (the plug) and water (the Aquarium).
  $n + {}^{1}H \rightarrow {}^{2}H + \gamma$ (2.22 MeV)

- The peak at 2.61 MeV corresponds to the de-excitation of $^{208}Pb^*$ as the last step in the Th-series (present in the concrete making up the walls of the experiment hall).
  ... $^{208}Tl \rightarrow e^- + \bar{\nu}_e + {}^{208}Pb^* \rightarrow {}^{208}Pb + \gamma$ (2.61 MeV)

- The peak at 4.44 MeV corresponds to the de-excitation of the first excited state of ^{12}C.
  $\alpha + {}^{9}Be \rightarrow {}^{12}C^* \rightarrow {}^{12}C + \gamma$ (4.44 MeV)

  - The peaks at 3.44 MeV and 3.95 MeV correspond to 4.44 MeV "double" escape and "single" escape peaks, respectively (see below).

If the incident gamma-ray has an energy above 1.022 MeV, the detector can register two extra peaks because pair-production[1] results in the creation of two 0.511 MeV e^+ e^- annihilation gamma-rays. If one of these gamma-rays is completely absorbed by the detector while the other one escapes, 0.511 MeV will be lost, and a so-called "single-escape peak" can be identified. If both annihilation gamma-rays escape, the "double-escape peak" results [25].

[1]Pair production is the spontaneous creation of an electron and a positron from a gamma-ray in field of an atomic nucleus.

3.2 ^{3}He-based Neutron Detector

3.2.1 Calibration

The spectra obtained using the ^{3}He detector are well-understood and the detector itself is considered to be self-calibrating. Recall Fig. 2.7. Three calibration points are used: the full-energy peak and the two edges corresponding to the wall effect. Figure 3.6 illustrates the energy calibration of the ^{3}He detector. As before, the peak energies have been plotted versus the peak positions for the each calibration point. A linear function was then fitted to these data. Referring to Eq. 3.1, the m value was determined to be $0.0009806 \frac{\text{MeV}}{\text{channel}}$ and b was determined to be 0.009241 MeV. By applying this calibration relation to all of our subsequent ^{3}He data, energy calibrated spectra were obtained (see Fig. 3.7).

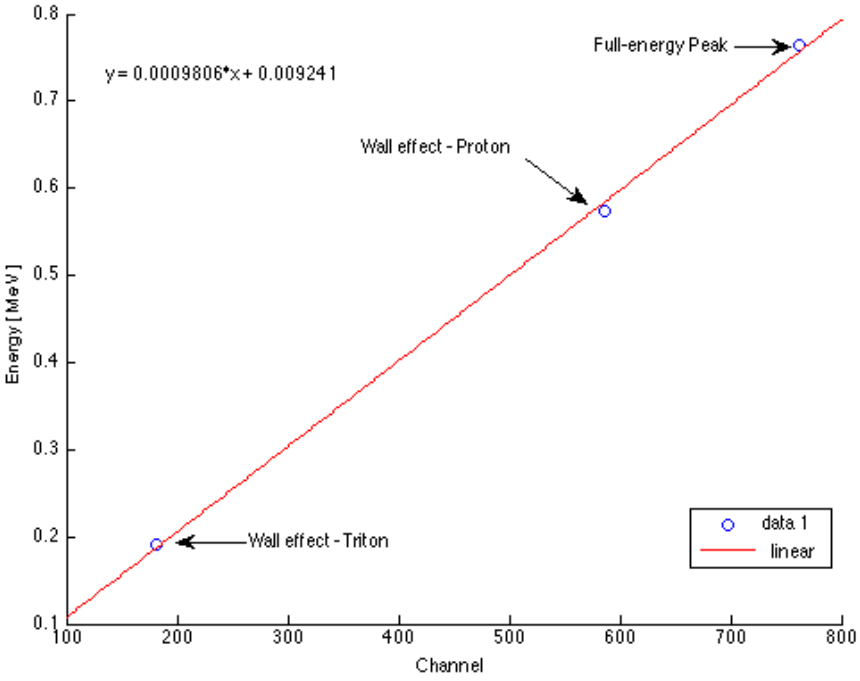

Figure 3.6: Energy calibration of the ^{3}He Detector. The energies of the three calibration points are plotted against the corresponding peak positions (open blue circles). A linear fitted energy-calibration relation (red line) is also shown.

3.2.2 Resolution

Energy resolution is not an issue for the measurements performed with the ^{3}He detector as the information about the energy of the incident neutron is lost to the nuclear reaction producing the p and ^{3}H.

3.2.3 Be-based Source Neutron Footprint

As previously mentioned, the detector was positioned 85 mm from the edge of the Aquarium and the height varied between the park and production positions. In some cases, a polyethylene plug was used to attenuate the Be-based source field. The first measurement involved determining the background radiological conditions within the room without the source. The measurements listed in Table 3.5 were then performed. Typical spectra are shown in Fig. 3.7.

Table 3.5: Measurements – ^{3}He Detector. Various source/detector geometrical configurations were investigated.

Run	Source Location	Detector Location	Plug
1	Production	Park	yes
2	Production	Park	No
3	Park	Park	No
4	Park	Production	No
5	Park	Production	Yes
6	Production	Production	Yes
7	Production	Production	No

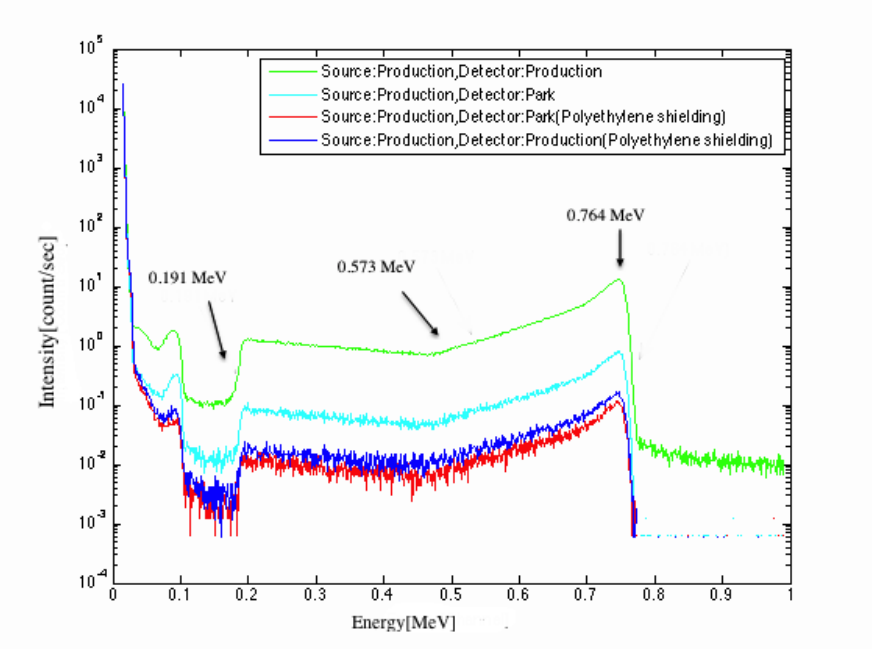

Figure 3.7: Calibrated ^{3}He Detector Energy Spectrum. Time-normalized, energy-calibrated neutron spectrum obtained using the Be-based source and the ^{3}He detector.

3.3 Rates

Using the calibrated detectors, the neutron and 4.44 MeV gamma-ray rates were obtained.

3.3.1 4.44 MeV Gamma-ray Rates

The rate of 4.44 MeV gamma-rays for each source and detector configuration with and without the polyethylene plug was determined by integrating the number of counts in the region of interest which included the 4.44 MeV peak and both the corresponding single- and double-escape peaks. Fig. 3.8 illustrates this region of interest. In all cases, the reported rates have been corrected for room background.

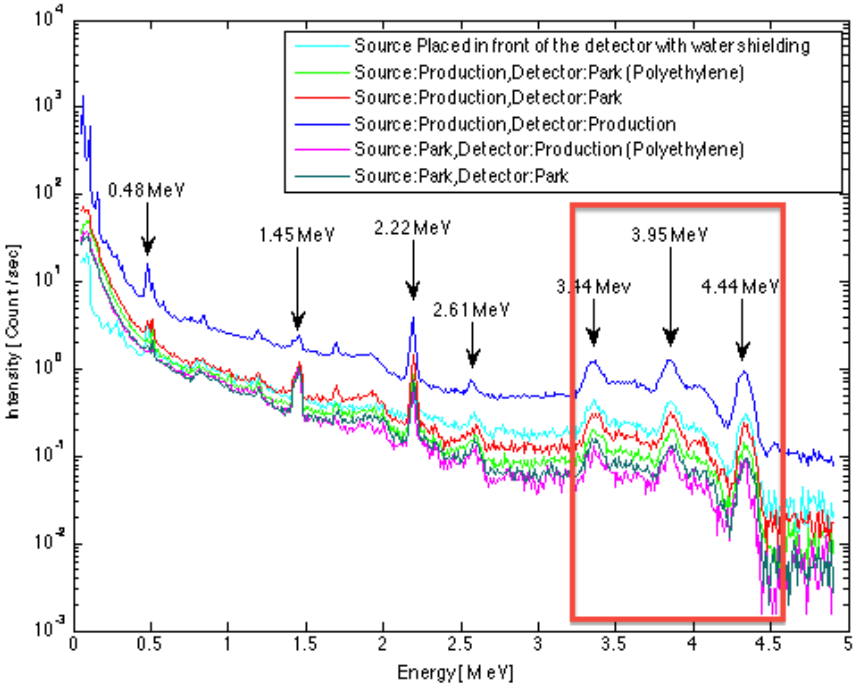

Figure 3.8: 4.44 MeV Gamma-ray Rates in the $LaBr_3(Ce)$ Detector. Time-normalized, energy-calibrated gamma-ray spectra obtained using the Be-based source and the $LaBr_3(Ce)$ detector in various configurations. The rate of 4.44 MeV gamma-rays was calculated from the number of counts in the red box, which includes the 4.44 MeV peak and both the single- and double-escape peaks.

Table 3.6 lists the measured rates of 4.44 MeV gamma-rays. It can clearly be seen that the measured rate of 4.44 MeV gamma-rays was a strong function of the amount of shielding between the source and the detector. The highest rate was observed when both the source and the detector were in production position and there was a clear line-of-sight between

them. The lowest rate was observed when the source was in park position, the detector was in production position, and the polyethylene plug blocked the penetration.

Table 3.6: Measured rates of 4.44 MeV Gamma-rays. The Be-based source and $LaBr_3(Ce)$ detector were in various configurations.

Source Location	Detector Location	Polyethylene Plug	Rate [Hz]	Fig. 3.9	Comment
Park	Production	Yes	7.1		
Park	Park	No	9.1	(b)	70 cm water
Production	Production	No	83.9	(a)	
Production	Park	No	19.9		
Production	Production	Yes	16.9		
Production	Park	Yes	12.9		

As a systematic check, we decided to confirm our 4.44 MeV gamma-ray results for the production/production (b) and park/park (a) configurations using the technique illustrated in Fig. 3.9. First, the $LaBr_3(Ce)$ detector was well-shielded from room background with lead and set at the height of the Be-based source with the same distance between the source and the detector as in the previous measurements (78.5 cm). A penetration in the lead shielding having approximately the same area as an Aquarium penetration was left, and a direct irradiation was performed (see Fig. 3.9 (a)). Then, two water jugs (each approximately 25 cm thick) were used to break line of sight between the source and the $LaBr_3(Ce)$ detector. Another irradiation was performed (see Fig. 3.9 (b)). We anticipated the 4.44 MeV gamma-ray rates measured with these configurations to be approximately the same as those measured using the Aquarium, and they were. The differences in the Park/Park measured rates, 9.1 Hz (Aquarium) versus 27.7 Hz (water jugs), are simply due to the extra 20 cm of water shielding breaking line-of-sight for the Aquarium measurement. See Table 3.7 for details.

Table 3.7: Confirmation of Measured Rates of 4.44 MeV Gamma-rays. See Fig. 3.9.

Shielding	Emulates	Fig. 3.9	Rate [Hz]	Comment
None	Production/Production	(a)	79.6	
Two water jugs	Park/Park	(b)	27.7	50 cm water

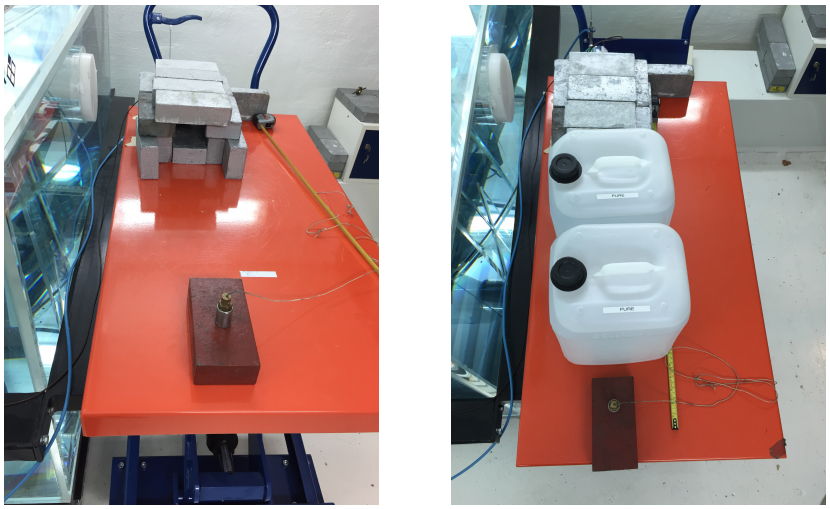

(a) (b)

Figure 3.9: Confirmation Measurement: The Source and $LaBr_3(Ce)$ Detector. The detector was well-shielded from room background by lead. (a) direct irradiation; (b) line-of-sight broken by two water jugs. Photographs by author.

3.3.2 Neutron Rates

Neutron rates were determined from the ^{3}He detector data by integrating the measured distributions between the full-energy peak at 0.764 MeV and the ^{3}H wall-effect shoulder at 0.191 MeV (see Fig. 3.10).

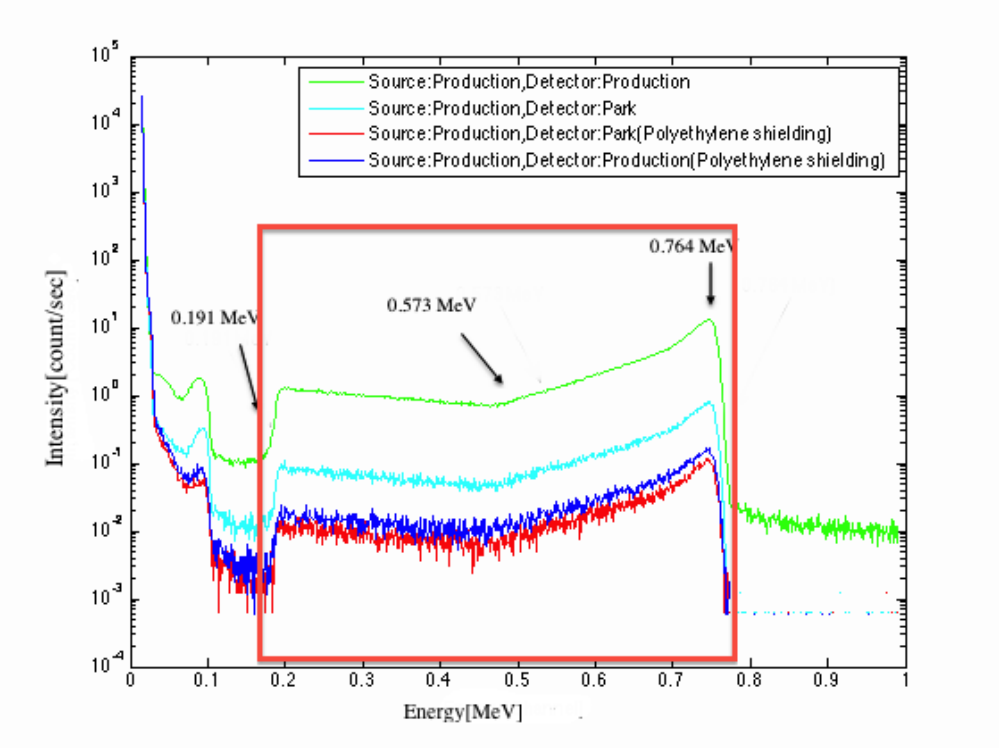

Figure 3.10: Neutron Rates in the ^{3}He Detector. Time-normalized, energy-calibrated neutron spectra obtained using the Be-based source and the ^{3}He detector. The rate of neutrons in the range of (0.191 – 0.764) MeV was calculated by integrating the distribution between the full-energy peak and the ^{3}H wall-effect shoulder, which is marked with a red box.

Table 3.8 lists the measured neutron rates. It can clearly be seen that the measured rate of neutrons was a strong function of the amount of shielding between the source and the detector. The highest rate was observed when both the source and the detector were in production position and there was a clear line-of-sight between them. The lowest rate was observed when the source was in park position, the detector was in production position, and the polyethylene plug blocked the penetration.

Table 3.8: Measured Neutron Rates. The Be-based source and ^{3}He detector were in various configurations.

Source Position	Detector Position	Polyethylene Plug	Rate [Hz]
Production	Production	No	430.0
Production	Park	No	28.2
Production	Production	Yes	5.8
Production	Park	Yes	3.7
Park	Production	No	108.0
Park	Park	No	5.1
Park	Park	Yes	0.4
Park	Production	Yes	0.4

No systematic check was performed on our neutron results. This was because our measurements were performed in an enclosed space so that neutrons could easily bounce off the walls and back into our detector in a less-than-obvious manner. This is in contrast to gamma-rays which tend to travel in straight lines.

Chapter 4

Conclusion

The purpose of this project was to perform a first investigation of the radiological footprint of a Be-based neutron source within the Aquarium of the STF at the Division of Nuclear Physics at Lund University. Neutron and gamma-ray energy spectra and count rates have been measured at Aquarium beamport apertures using ^{3}He and $LaBr_3$(Ce) detectors with very simple cylindrical geometries. These spectra and rates will serve as benchmarks for ongoing efforts to simulate the neutron and gamma-ray fields associated with the source. The development of a software toolkit which precisely reproduces the radiological environment will in turn facilitate the interpretation of detector-development and shielding studies performed at the STF.

4.1 $LaBr_3$(Ce) Gamma-ray Detector

The $LaBr_3$(Ce) gamma-ray detector was successfully calibrated using gamma-ray sources. These gamma-ray sources included ^{60}Co, ^{137}Cs, and ^{22}Na. The intrinsic activity of ^{138}La provided another calibration point. A linear energy-calibration relation was determined from the calibration measurements. This calibration relation was then employed to examine the gamma-ray footprint of the room and the Be-based source. Room-associated gamma-rays included those from the de-excitation of ^{208}Pb* as the last step in the Th-series. Be-based source-related gamma-rays included those from the capture of neutrons on ^{1}H (present in the water in the Aquarium and the polyethylene plug), ^{10}B (present in the plastic of the detector support), and ^{12}C (from the source itself). These data were also employed to establish the energy resolution of the detector over the range (0.511 - 4.44) MeV at (3.9 $\pm$ 0.3)%. Finally, the rate of 4.44 MeV gamma-rays (which included both the single-escape and double-escape peaks) was extracted from the data for different types and thicknesses of shielding between the detector and the source. Both water and polyethylene were determined to be effective shielding materials against 4.44 MeV gamma-rays as the measured rates dropped substantially as the shielding thickness increased. Each material has benefits and drawbacks, but the fire-resistant aspect of water shielding in combination with a Be-based source is certainly a plus.

4.2 ^{3}He-based Neutron Detector

The ^{3}He-based neutron detector was successfully calibrated using the Be-based source. The calibration employed the shoulders due to the wall effect together with the full-energy peak. A linear energy-calibration relation was determined from the calibration measurements. This calibration relation was then employed to examine the neutron footprint of the room and the Be-based source. Energy resolution was not an issue as the information about the incident neutron energy is lost to the reaction used to detect it. Room-associated neutrons were negligible. Be-based source-related neutrons were plentiful. Note that the neutrons emitted by the Be-based source were fast; that is, they had energies on the order of about 5 MeV. The ^{3}He-based neutron detector was largely sensitive to thermal neutrons. The rate of thermal neutrons was extracted from the data for different types and thicknesses of shielding between the detector and the source. Both water and polyethylene were determined to be effective shielding materials against 5 MeV neutrons as the shielding thicknesses increased. However, in this case, not all of the fast neutrons were stopped by the shielding. Instead, sometimes the shielding acted only to slow down the neutrons and thus make them easier to detect with the ^{3}He-based neutron detector. Thus, it is not clear that a ^{3}He-based detector is the single best choice for investigating the neutron footprint of a Be-based source. In order to improve the measurements of the source-associated neutron rates, the series of experiments should be redone with a fast-neutron detector in order to provide more information for the simulations.

Bibliography

[1] Neutrons. Wikipedia. [accessed May 7, 2015]. http://en.wikipedia.org/wiki/Neutron

[2] Isitelps: Nuclear Chemistry online. Sean M. Putnam. [accessed May 3, 2015]. http://isite.lps.org

[3] Nuclear Stability online. [accessed May 3, 2015]. http://physics.tutorvista.com/modern-physics

[4] K. Nakamura and the Particle Data Group, Review of Particle Physics, Journal of Physics G: Nuclear and Particle Physics, vol. 37, no. 7A, p. 075021 (2010). http://stacks.iop.org/0954-3899/37/i=7A/a=075021

[5] K. Heyde, "Basic Ideas and Concepts in Nuclear Physics: An Introductory Approach", Third Edition (2004). ISBN 9780750309806 - CAT IP157.

[6] Geant4: application online. [accessed May 16, 2015]. http://geant4.cern.ch/

[7] MCNPX: application online. [accessed May 16, 2015]. https://mcnpx.lanl.gov/

[8] McStas: application online. [accessed May 16, 2015]. http://www.mcstas.org/

[9] R.A. Cecil, B.D. Anderson, R. Madey, "Improved Predictions of Neutron Detection Efficiency for Hydrocarbon Scintillators from 1 MeV to about 300 MeV", Nuclear Instruments and Methods, vol. 161, p. 439 (1979). DOI: 10.1016/0029-554X(79)90417-8.

[10] H.R. Vega Carrillo, V.M. Hernndez-Dvila, T. Rivera-Montalvo, A. Snchez, "Characterization of a 239PuBe Isotopic Neutron Source", Proceedings of the ISSSD (2012). ISBN 978-607-00-6167-7.

[11] S.Notarrigo, F.Porto, A.Rubbino, S.Sambataro, "Experimental and Calculated Energy Spectra of Am-Be and Pu-Be Neutron Sources", Nuclear Physics A, vol. 125, p. 28 (1969). DOI: 10.1016/0375-9474(69)90826-4.

[12] Supplied by High Tech Sources Limited. [accessed May 6, 2015]. http://www.hightechsource.co.uk

[13] CAD drawings by H. Svensson from the Mechanical Engineering Division of the MAX IV Lab.

[14] VINK AS. [accessed May 10, 2015]. http://vink.se

[15] G. F. Knoll, "Radiation Detection and Measurement", Fourth Edition (2010). ISBN: 978-047-01-3148-0.

[16] [accessed May 14, 2015]. http://www.kip.uni-heidelberg.de/ coulon/Lectures/Detectors/

[17] [accessed May 14, 2015]. http://www.et-enterprises.com/photomultipliers/understanding-photomultipliers/

[18] [accessed May 15, 2015]. http://www.qorpak.com/WhatisBorosilicateGlass.aspx

[19] Elijen Technology: Product catalog online. [accessed May 17, 2015]. http://www.eljentechnology.com/index.php/products/

[20] ORTEC. Lanthanum Bromide Scintillation Detectors: Product catalog online. Lanthanum Bromide Scintillation Detectors. [accessed May 5, 2015]. http://www.ortec-online.com

[21] E. V. D. van Loef, P. Dorenbos, C. W. E. van Eijk, K. W. Kraemer and H. U. Guedel, "High-energy-resolution scintillator: Ce3+ activated LaBr3", Applied Physics Letters, vol. 79, p. 1573 (2001). DOI: 10.1063/1.1385342.

[22] J. E. Ellsworth, "Post He-3 Neutron Detection at BYU", 2010.

[23] M. Das, "Impulse function - Dirac Delta in scilab". http://www.equalis.com/blogpost/731635/139333/Impulse-function–Dirac-Delta-in-scilab. Tuesday, February 28, 2012.

[24] [accessed May 17, 2015]. http://www.mt.mahidol.ac.th/e-learning/Instrumentation/

[25] C.S. Park, G.M. Sun, H.D. Choi, "Determination of Single Escape and Double Escape Peak Efficiency for a HPGe Detector", Journal of the Korean Nuclear Society, vol. 35, no. 6, p. 523 (2003).

Appendix A

Contribution of the Author

Table A.1: Week-by-Week Summary. The contribution of the author to this project.

Week	Activity
3	Background reading
4	Background reading
5	Background reading
6	Background reading
7	Radiation Course Jefferson Lab DOE Radiation Worker 1, DNPLU walkthrough
8	Familiarize with equipment
9	Familiarize with equipment
10	Experiment ($LaBr_3$(Ce) Detector, using the calibration sources)
11	Experiment (^{3}He detector)
12	Analysing data set 1
13	Experiment ($LaBr_3$(Ce) Detector, using the Be-based sources)
14	Analyzing data set 2
15	Analyzing data set 2
16	Repeat the experiment by using $LaBr_3$(Ce) detector
17	Analyzing data set 3
18	Repeat experiment using $LaBr_3$(Ce) detector and analyzing data set 4
19	Writing of thesis
20	Writing of thesis
21	Writing of thesis

Appendix B

Self Reflection

During the past five months, I have been involved in the work described in this thesis, which was the first benchmark measurements of neutron and gamma-ray energy spectra at the STF obtained using ^{3}He neutron and cerium-activated lanthanum bromide ($LaBr_3(Ce)$) gamma-ray detectors. It was a great experience to work with Dr. Kevin Fissum and his group. I gained a lot of hands-on experience along with learning new programming skills. I had not taken any nuclear physics class and I thought I was not prepared for a project in the field. However, everyone was truly patient and helped me along the way and made it a great experience for me. We had several unsuccessful measurements and had to repeat the experiment, but I learned something new every time we repeated the experiment. All in all, this project has provided me with valuable research experience which I am certain will be useful in my future studies.

The project reported upon in this thesis
was performed in collaboration with

The Source-based Neutron Irradiation Group
of the Division of Nuclear Physics at Lund University

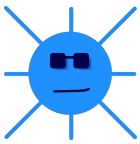

and the

The Detector Group of the European Spallation Source